Adsorption of methylene blue by using novel chitosan-g-itaconic acid/bentonite nanocomposite – equilibrium and kinetic study

Farzaneh Shakib, Ahmad Dadvand Koohi and Arash Kamran Pirzaman

ABSTRACT

In this study, novel chitosan-g-itaconic acid/bentonite (CTS-g-IA/BT) and chitosan/bentonite (CTS/BT) nanocomposites were synthesized for adsorption of methylene blue (MB) from aqueous solution. The process was pH-sensitive and maximum sorption was obtained at pH 6 (CTS-g-IA/BT) and 7 (CTS/BT) in 76 h agitation time using 0.03 g of nanocomposites for 50 mL of MB solution. The results showed that in pH less than 6, the adsorption capacity of CTS-g-IA/BT nanocomposite due to the existence of IA monomer is less than that of CTS/BT nanocomposite. The Fourier transform infrared spectroscopy (FTIR) spectrum of CTS-g-IA/BT revealed that both itaconic acid and BT present in the nanocomposite structure, and also the –OH groups of BT, $–NH_2$ and –OH of CTS participated in nanocomposite formation. According to the FTIR results, a schematic diagram of the nanocomposite synthesis was presented. The kinetic results indicated that the adsorption of MB fitted well with the pseudo-second-order kinetic model. The equilibrium data followed Langmuir isotherm with the maximum adsorption capacity of 500 and 181.818 mg/g for CTS-g-IA/BT and CTS/BT nanocomposites, respectively. The negative values of Gibbs free energy change (ΔG^0) and the positive values of ΔH^0 confirmed that the adsorption process is spontaneous and endothermic. The positive values of ΔS^0 suggested the randomness of adsorption at interface.

Key words | bentonite, chitosan, itaconic acid, methylene blue, nanocomposite

Farzaneh Shakib
Arash Kamran Pirzaman
Chemical Engineering Department, Engineering Faculty,
University of Science and Technology of Mazandran,
Behshahr,
Iran

Ahmad Dadvand Koohi (corresponding author)
Chemical Engineering Department, Engineering Faculty,
University of Guilan,
Rasht,
Iran
E-mail: *dadvand@guilan.ac.ir*

INTRODUCTION

Synthetic dyes are employed in many industries like printing, plastic, textile, paper and food. Because of the harmful effects of dyes on both humans and the environment, the industries' effluent must be treated (Liu *et al.* 2010). Various methods have been developed so far for treating industrial wastewater, including membrane separation (Tahri *et al.* 2012), electro coagulation (Merzouk *et al.* 2010) and adsorption (Salama *et al.* 2014). Among the several techniques for removal of dyes, adsorption has been found as a facile, economical, cheap and effective method (Kaplan & Kasgoz 2011). Many efforts have been made to find an appropriate adsorbent. Polymeric adsorbents enable to adsorb anionic and cationic pollutants such as dyes and metal ions. Polymeric hydrogels are crosslinked, hydrophilic, three-dimensional networks with functional groups that can adsorb wastewater pollutions. Due to their abundant resources, biodegradability, low cost, low toxicity, and environmentally friendly natures, they have attracted special research attention (Bao *et al.* 2011; Pourjavadi *et al.* 2015). Generally, hydrogels are obtained from biopolymers such as chitosan (CTS) (Moussout *et al.* 2016), starch (Guclu *et al.* 2010), collagen (Kurdtabar *et al.* 2015), guar gum (Sharma *et al.* 2015) and cellulose (Liu *et al.* 2010). CTS is a linear biopolymer, which is prepared by deacetylation of chitin, and is the second most abundant polymer in the world after cellulose. CTS is an effective adsorbent for removal of dye and metal ions due to the presence of hydroxyl and amino functional groups. The pollution adsorption property of CTS, along with its non-toxicity and biodegradability, has made it useful for environmental applications (Auta & Hameed 2014). Nowadays, grafting functional groups like carboxyl and sulfonic groups on the polysaccharide backbone can improve adsorption capacity and adsorption rate; this is done by grafting acrylamide (AM) (Yang & Ni 2012), acrylic acid (AA) (He *et al.* 2012) and 2-acrylamido-2-methylpropane

doi: 10.2166/wst.2017.077

sulfonic acid (AMPS) (Bao *et al.* 2011). Because of double carboxylic acid groups of itaconic acid, it can be used to improve adsorption capacity in removal of cationic dyes from aqueous solutions (Kaplan & Kasgoz 2011). Thus, special attention has been paid to hydrogels due to their different functional groups and high adsorption capacity.

Lately, because of the poor mechanical strength of polymeric hydrogels, an inorganic component like smectite group clay mineral was added into the polymer matrix to improve their properties. Therefore, enjoying superior properties, nanocomposites are better than pure polymers and hydrogels (Liu *et al.* 2010; Wang *et al.* 2014). Different clay minerals were used to prepare nanocomposites like bentonite (BT) (Wang *et al.* 2014), attapulgite (Liu *et al.* 2010), rectorite (Zheng & Wang 2009) and montmorillonite (Wang *et al.* 2008). Among the different clays, BT is a natural clay consisting of two tetrahedral silicate sheets with an alumina octahedral sheet in the center of each layer and exchangeable cations between the layers (Shirsath *et al.* 2011). Shirsath *et al.* (2011) reported the synthesis of poly (acrylic acid)-BT-FeCo nanocomposite for removal of crystal violet. The addition of BT clay into the nanocomposite structure enhanced the strength of nanocomposites.

Therefore, it seems that combining the biopolymers with monomer (e.g. itaconic acid) and clay (e.g. BT) can improve the dye adsorption capacity and the strength of nanocomposites. In this work, new nanocomposites were prepared with CTS biopolymer, itaconic acid monomer and BT clay for methylene blue (MB) adsorption from aqueous solutions. N,N'-methylenebisacrylamide (MBA) and ammonium persulfate (APS) were used as crosslinker and initiator, respectively. The adsorption of MB under different experimental conditions such as pH of the initial solution, adsorbent amount and contact time was studied. Lastly, the adsorption kinetics, isotherms and thermodynamic parameters were also investigated.

MATERIALS AND METHODS

Materials

BT and CTS from shrimp shells were obtained from Sigma-Aldrich Company. APS, MBA and itaconic acid (methylenesuccinic acid-IA) were purchased from Merck. MB, HCl and NaOH were also obtained from Merck. The MB stock solution was prepared by dissolving MB in deionized water to the concentration of 1,000 mg/L. Working solutions were prepared by diluting the stock dye solutions to the required concentrations. HCl and NaOH (1M) were used to adjust the initial pH of the dye solution.

Preparation of CTS-g-IA/BT and CTS/BT nanocomposites

First, to eliminate the dissolved oxygen, deionized water was purged with nitrogen gas for 5 min. 1 g of CTS powder was added to 50 mL of acetic acid 1% (v/v) to prepare CTS solution in a 250 mL flask. The solution was stirred until CTS dissolved completely. Next, 10 mL of BT solution (2 wt%) was added under continuous stirring to reach a homogenous solution. The homogeneous solution of CTS-BT was heated up to 70 °C. Then, 0.02 g of APS initiator was added to the CTS-BT solution, and the solution temperature was maintained at 70 °C for 10 min to generate free radicals. The mixed solution of 1 g itaconic acid and 0.2 g MBA was added to the CTS-BT solution after cooling down the reactants to 40 °C for 10 min. The temperature was raised to 70 °C, and was kept at this condition for 3 h to complete the polymerization reaction. The product was dried at room temperature and then the nanocomposites were placed in excess amounts of deionized water to remove the unreacted molecules such as monomer, crosslinker and initiator for 3 days. The dewatered nanocomposites were dried at room temperature, and the dried adsorbents were used for the experimental studies. Itaconic acid was deleted from the previous method to prepare CTS/BT nanocomposite.

Methods

Adsorption studies

Adsorption experiments were done on a shaker (HeidolpH Unimax 1010) at a constant rate of 120 rpm with 0.03 g of adsorbent and 50 mL of MB solution of known pH and concentration. Concentration of the residual of MB in the solution was determined by a UV-Vis spectrophotometer (Cary 50 bio UV-visible) at a wavelength corresponding to the maximum absorbance, $\lambda max = 664$ nm for MB (Wang *et al.* 2008). The calibration curve between absorbance and MB concentration was plotted ($R^2 = 0.998$). The adsorption capacity at any time (q_t), and at equilibrium (q_e) was calculated by Equations (1) and (2), respectively:

$$q_t = \frac{C_0 - C_t}{m} \times V \quad (1)$$

$$q_e = \frac{C_0 - C_e}{m} \times V \quad (2)$$

where C_0 is the initial dye concentration (mg/L), C_t is the concentration at time t (mg/L), C_e is the equilibrium dye concentration (mg/L), m is the adsorbent mass (g), and V is the volume of the dye solution (L).

Equilibrium studies

An isotherm model describes the relation between the dye concentration in solution and the dye concentration on the surface of adsorbent at equilibrium conditions. To understand the surface properties and mechanism of adsorption, the adsorption isotherm models were investigated. The experimental data were fitted with several isotherm models, including Langmuir, Freundlich and Dubinin–Radushkevich (D-R). Comparison of the correlation coefficient (R^2) values determined the best fitness to the adsorption model. Adsorption of MB using CTS/BT and CTS-g-IA/BT nanocomposites was examined at three temperatures (25, 35 and 40 °C). Equilibrium studies were conducted using batch equilibrium technique. The 21 samples (0.03 g) of each nanocomposite (CTS-g-IA/BT and CTS/BT) were added to 50 mL of MB aqueous solution. These experiments were carried out with different initial concentrations (50, 75, 150, 200, 300 and 400 mg/L) and at the same three temperatures (25, 35 and 40 °C).

Langmuir isotherm

Langmuir equation assumes that the adsorbent surface is homogeneous; i.e. the adsorbent is able to adsorb one molecule. Therefore, the adsorption process will be monolayer, and there will be no interaction between adsorbate dye molecules on the surface of the adsorbent. All active sites have equivalent energies for adsorption. The linear form of Langmuir equation is represented as follows:

$$\frac{C_e}{q_e} = \frac{C_e}{q_m} + \frac{1}{K_L q_m} \tag{3}$$

The plot of the C_e/q_e versus C_e gives a straight line; q_m and K_L values can be determined from the slope and intercept of the plot, respectively. The feasibility of the adsorption process is expressed by separation factor (R_L), or equilibrium parameter as follows:

$$R_L = \frac{1}{1 + K_L C_0} \tag{4}$$

where C_0 is the initial MB concentration (mg/L), q_m is related to the maximum adsorption capacity (mg/g), and K_L is the Langmuir constant (L/mg). Favorability of Langmuir adsorption isotherm is determined by R_L value. $R_L = 0$ indicates irreversible adsorption, $0 < R_L < 1$ suggests favorable adsorption, $R_L = 1$ adsorption is linear, $R_L > 1$ represents unfavorable adsorption (Kumar & Tamilarasan 2013; Mittal *et al.* 2014).

Freundlich isotherm

Freundlich isotherm describes multilayer adsorption on a heterogeneous adsorbent surface where the heat of adsorption distributes non-uniformly; also, it is an empirical adsorption equation. The linear form of Freundlich equation is expressed as follows:

$$\ln q_e = \ln K_F + \frac{1}{n} \ln C_e \tag{5}$$

where K_F is Freundlich isotherm constant, and n is a dimensionless constant. $1/n$ and K_F values were determined from the slope and intercept of the plot of lnq_e versus lnC_e, respectively. The $1/n$ value can predict the feasibility of adsorbent in all ranges of concentration. If $1/n$ value is less than 1, the adsorbent can be employed in all investigated concentrations of adsorbate, and when $1/n$ value is greater than 1, adsorbent is only useful for higher studied concentrations (Mittal *et al.* 2014).

D-R isotherm

D-R isotherm can be described for both heterogeneous and homogenous surfaces. It can also be applied to predict the nature of adsorption process, whether the adsorption is a physical or chemical process (Liu *et al.* 2010). A linear form of the D-R equation is as below:

$$lnq_e = \ln(q_D) - K\varepsilon^2 \tag{6}$$

where q_D is the theoretical saturation capacity (mg/g), K is the D-R constant (mol^2/J^2), and ε is Polanyi potential, which is estimated by the following equation:

$$\varepsilon = RT\, ln\left(1 + \frac{1}{C_e}\right) \tag{7}$$

where R is the universal gas constant (8.314J/mol K), and T is the absolute temperature (K). From the slope and intercept of the plot between lnq_e and ε^2, K and q_D values are obtained, respectively. The mean adsorption energy

(J/mol) is calculated using the following expression:

$$E = (2K)^{-1/2} \tag{8}$$

The nature of adsorption process is determined by the mean adsorption energy (E). The E value between 8 and 16 kJ/mol indicates a chemisorption, and the process is a physical adsorption with an E value less than 8 kJ/mol (Dang *et al.* 2009).

Thermodynamic parameters

Thermodynamic parameters investigate the effect of temperature on adsorption process to find out the nature of the adsorption process. The thermodynamic parameters including the standard enthalpy change (ΔH^0, kJ/mol), the standard Gibbs free energy change (ΔG^0, kJ/mol) and the standard entropy change (ΔS^0, kJ/mol K) were examined in this study. The thermodynamic equilibrium constant is defined using the following equation:

$$K_0 = \frac{a_s}{a_e} = \frac{v_s q_e}{v_e c_e} \tag{9}$$

where a_s is the activity of the adsorbed MB, a_e is the activity of MB in the solution at equilibrium state, v_s is the activity coefficient of the adsorbed solute, and v_e is the activity coefficient of solute in solution at equilibrium. When the concentration of dye approaches zero, the activity coefficient approaches unity:

$$\lim_{C_{e\to 0}} \frac{q_e}{C_e} = \frac{a_s}{a_e} = K_0 \tag{10}$$

The value of K_0 can be determined by plotting $ln(q_e/c_e)$ against C_e, and extrapolating C_e to zero. In the present study, to obtain the thermodynamic parameters, temperature varied in the range of 25–40 °C. ΔG^0, ΔH^0 *and* ΔS^0 were evaluated using the following equations:

$$\Delta G^0 = -RTlnK_0 \tag{11}$$

$$Ln(K_0) = -\frac{\Delta H^0}{RT} + \frac{\Delta S^0}{R} \tag{12}$$

where R is the universal gas constant (8.314 J/mol K), and T is the absolute temperature (K). ΔH^0 and ΔS^0 were calculated from the slope and intercept of the linear plot of lnK_0 versus $1/T$ (Tabrizi & Yavari 2015; Wu *et al.* 2015).

Kinetic studies

Kinetic studies include investigation of how different experimental conditions can influence the rate of a reaction and yield information about the mechanism of reaction. Generally, predicting the rate of adsorption is an important factor in the design of a desirable adsorption process. For this purpose, 0.03 g of each adsorbent (CTS/BT and CTS-g-IA/BT nanocomposites) was put in a beaker containing 50 mL of 50 mg/L MB solution at optimum pH. The shaking was carried out under constant stirring at 120 rpm. For evaluating the adsorption rate, the experimental data were fitted to different models, including pseudo-first-order, pseudo-second-order and intraparticle diffusion.

Pseudo-first-order model

The linear form of pseudo-first-order model is given by:

$$\log(q_e - q_t) = \log(q_e) - \frac{k_1}{2.303} t \tag{13}$$

where q_e and q_t are the amount of MB absorbed at equilibrium time and at time t (mg/g), respectively, and k_1 is the rate constant of first-order sorption (1/min). Plotting $log(q_e\text{-}q_t)$ against time gives q_e and k_1 values (Liu *et al.* 2010; Fu *et al.* 2015).

Pseudo-second-order model

Pseudo-second-order model can be written as follows:

$$\frac{t}{q_t} = \frac{1}{k_2 q_e^2} + \frac{1}{q_e} t \tag{14}$$

where k_2 is the pseudo-second-order adsorption rate constant (g/mg min), and q_e and q_t are the adsorption capacity at equilibrium and at time t (mg/g), respectively. q_e and k_2 can be computed from the slope and intercept of the straight line obtained from plotting t/q_t against t (Liu *et al.* 2010; Fu *et al.* 2015).

Intraparticle diffusion model

Intraparticle diffusion model can identify the limiting step of the rate of adsorption process that includes transfer of adsorbate from the bulk solution to the internal surface of adsorbent; thus, the mechanism of adsorption is

determined. Weber's intraparticle diffusion model is written as below:

$$q_t = k_i t^{0.5} + I \tag{15}$$

where k_i is the intraparticle diffusion rate constant (mg/g $min^{0.5}$), and I is the boundary layer thickness (mg/g) that indicates the resistance of mass transfer in the external liquid film. Plotting q_t versus $t^{0.5}$ gives k_i and I from the slope and intercept of the straight line. If the plot is a straight line and passes through the origin, the intraparticle diffusion model is a rate limiting step, but if plotting q_t versus $t^{0.5}$ includes multi-linear, it found that film-diffusion or chemical reaction controls the adsorption rate. Previous research has indicated that the plot usually presents multi-linear, showing that, generally, adsorption process may be controlled by more steps like film diffusion, intra particle diffusion, and chemical reaction (Aflaki Jalali *et al.* 2016).

RESULTS AND DISCUSSION

Fourier transform infrared spectroscopy

The Fourier transform infrared spectroscopy (FTIR) spectra of CTS (a), IA (b), BT (c), CTS-g-IA/BT (d), and CTS/BT (e) are shown in Figure 1. In the spectrum of CTS (Figure 1(a)), the broad band in the range of 3,000–3,500 cm^{-1} is related to O–H stretching vibration. The bands at 3,436 and 2,883 cm^{-1} are related to N–H and C–H stretching vibrations, respectively. The absorption band in the range of 1,647–1,694 cm^{-1} can be attributed to the C=O remainder of raw material. The absorption peaks at 1,558, 1,387–1,427 and 1,214 cm^{-1} are $-NH_2$, $-CH_2$ and C–N bending vibrations, respectively. The stretching vibration of C–OH is seen at 1,081 cm^{-1} (Milosavljevic *et al.* 2010).

In the spectrum of itaconic acid (Figure 1(b)), the broad band in the range of 2,500–3,500 cm^{-1} is due to O–H stretching vibration. The band at 1,707 cm^{-1} is related to the C=O

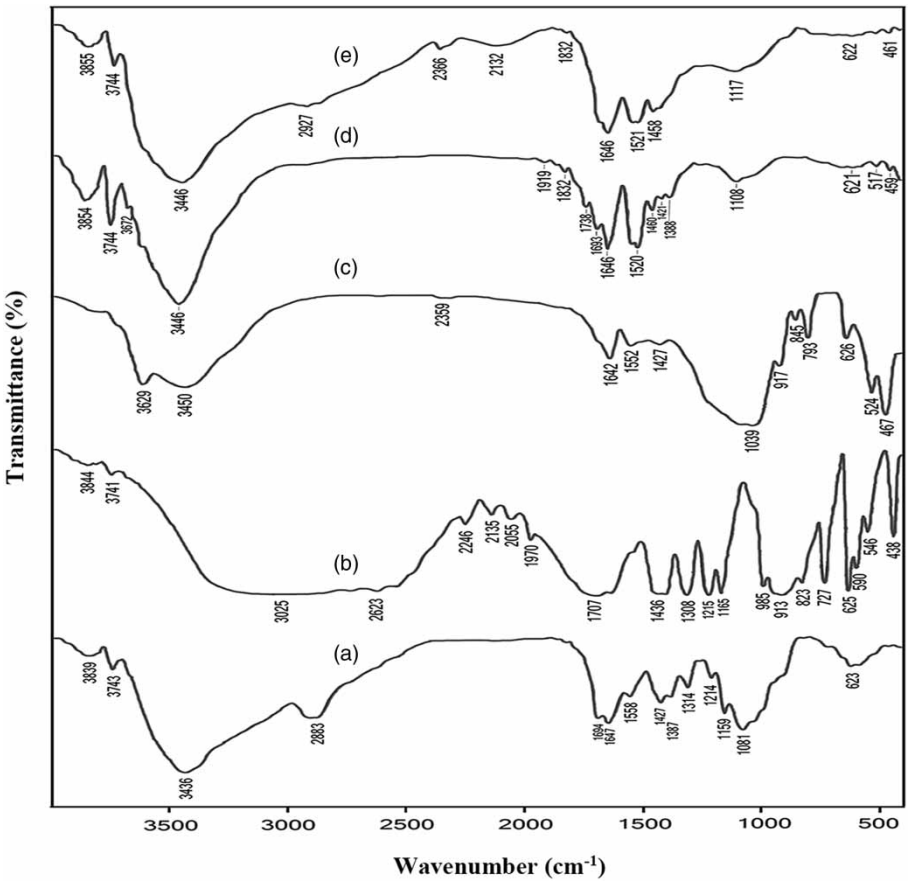

Figure 1 | The FTIR spectra of CTS (a), IA (b), BT (c), CTS-g-IA/BT nanocomposite (d) and CTS/BT nanocomposite (e).

asymmetric stretching vibration of carboxylic acid (–COOH) groups. Stretching vibration of C=C bond is observed at 1,650 cm^{-1}, and bending vibration of C-H in the –CH and $–CH_2$ groups is observed in the range of 1,308–1,436 cm^{-1}. The C=O symmetric stretching vibration of carboxylic acid (–COOH) groups appeared at 1,436 cm^{-1}. The absorption band in the 1,165–1,215 cm^{-1} region can be attributed to C-O stretching vibration and the bending vibration of $=CH_2$ is observed at 913 cm^{-1} (Shivarkar *et al.* 2015). In the spectrum of BT (Figure 1(c)), the stretching vibration of Al-Al-OH is found at 3,629 cm^{-1}. The absorption band at 2,500–3,500 cm^{-1} is because of the O-H stretching of the adsorbed water. The bands at 1,642, 917 and 626 cm^{-1} are attributed to the O-H of bending vibration of the adsorbed water, Al-Al-OH and Si-O bending vibrations, respectively. The bands at 524 and 467 cm^{-1} are due to the Si-O-Al and Si-O-Mg tetrahedral bending modes (Wang *et al.* 2014).

Comparing the FTIR spectrum of CTS-g-IA/BT nanocomposite (Figure 1(d)) with those of CTS, IA and BT shows that the stretching vibration of N-H, which confirms the existence of MBA and APS into the CTS-g-IA/BT nanocomposite, overlaps with the O-H stretching vibration at 3,446 cm^{-1}. The new absorption peak at 1,738 cm^{-1} is ascribed to the C=O stretching vibration of the carboxylic acid (–COOH) groups, and the new peaks at 517 and 461 cm^{-1} are related to Si-O-Al and Si-O-Mg of tetrahedral bending mode, confirming the existence of BT into the CTS-g-IA/BT nanocomposite. On the other hand, by comparing the FTIR spectrum of CTS/BT nanocomposite (Figure 1(e)) with those of CTS and BT, it is observed that the stretching vibration of N-H, which confirms the existence of MBA and APS into the CTS/BT nanocomposite, overlaps with the O-H stretching vibration at 3,446 cm^{-1}. The new peak at 461 cm^{-1} is related to Si-O-Mg of tetrahedral bending mode that shows the existence of BT into the CTS/BT nanocomposite. In the spectra of CTS-g-IA/BT and CTS/BT, disappearing of absorption band at 3,629 cm^{-1}, which is related to the –OH groups in BT, indicates participation of the –OH groups in polymerization. Also, the absorption bands of $–NH_2$ and –OH (1,558 and 1,081 cm^{-1}) of CTS have disappeared in the CTS-g-IA/BT and CTS/BT nanocomposites, indicating the participation of these groups in graft polymerization (Zhang *et al.* 2007; Kaplan & Kasgoz 2011). As a result, we can conclude that BT and itaconic acid participate in the grafting polymerization reaction. A schematic diagram of nanocomposite synthesis is illustrated in Figure 2.

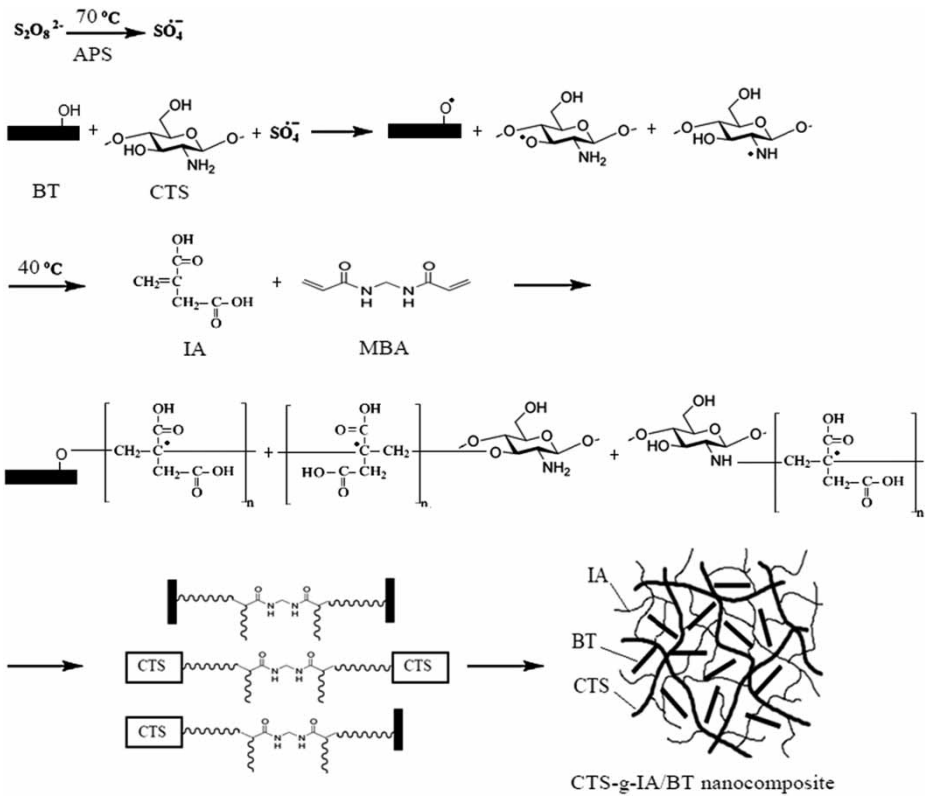

Figure 2 | Schematic diagram of CTS-g-IA/BT nanocomposite.

Effects of pH on adsorption

Usually, the initial pH of the solution has the most effect on the adsorption process, and plays a significant role to obtain the adsorbate degree of ionization. For this purpose, the adsorbents (0.03 g) with 50 mg/L of initial dye concentration and 50 mL of solution were tested. The experimental results for MB adsorption onto CTS-g-IA/BT and CTS/BT nanocomposites in the pH range of 3–9 are shown in Figure 3. The synthesized anionic nanocomposites, including the hydroxyl and carboxyl functional groups, were affected by the pH of the dye solution. As shown the adsorption capacity of CTS-g-IA/BT nanocomposite is very low in high acidic pH (less than 10 mg/g) because the carboxyl and hydroxyl functional groups are mostly in non-ionized (-OH, -COOH) form and a low interaction can occur between the cationic dyes and these groups (Guclu *et al.* 2010); also the H^+ ions existing in the solution compete with the cationic MB for negative sites of the adsorbents like carboxylic acid. Thus, it is difficult for MB molecules to diffuse on the adsorbent surface (Liu *et al.* 2010); hence, the adsorption capacity is reduced. The adsorption capacity increase with the increase of pH value, and the maximum adsorption capacity is obtained in pH = 6 and pH = 7 for CTS-g-IA/BT and CTS/BT nanocomposites, respectively. At these pH values, the carboxyl and hydroxyl functional groups of nanocomposites dissociate. Therefore, these groups are present in $–O^-$ and $–COO^-$ form in nanocomposites, and strong electrostatic interactions could occur between the positive site of MB and the negative site of adsorbent. Likewise, at pH values higher than 7, there was a little decrease in the adsorption that could be related to the existence of a large amount of Na^+ in the MB solution medium prevented interactions between MB and the anionic functional group of adsorbent (Liu *et al.* 2010; Auta & Hameed 2014). By more accurate investigation of Figure 3, it can be seen that in acidic condition (pH = 3–5), the adsorption capacity of CTS-g-IA/BT nanocomposite is less than that of CTS/BT nanocomposite. This could be due to the fact that in acidic condition, functional groups are in non-ionic form, and thus have little role in the adsorption. In CTS-g-IA/BT nanocomposite, the layers of BT are filled with IA monomers; however, in CTS/BT nanocomposite, no IA monomers are present across the BT layers; therefore, cation exchange reaction between BT layers and MB can take place simply in CTS/BT nanocomposite and not in CTS-g-IA/BT. Hence, pH = 6 and pH = 7 were considered as the optimum pH for CTS-g-IA/BT and CTS/BT nanocomposites, respectively, for further experiments.

Effect of adsorbent amount on adsorption

Since the amount of adsorbent reduces adsorption process expense, it can be a very important factor in selection of a suitable adsorbent. An adsorbent, which can remove a large amount of adsorbate at low adsorbent dose, is a favorable adsorbent (Aflaki Jalali *et al.* 2016). The experiments were carried out using different amounts of adsorbent in the range of 0.01–0.07 g, 50 mg/L of initial MB concentration, 50 mL of MB solution, and pH 6 and 7 for CTS-g-IA/BT and CTS/BT nanocomposites, respectively (Figure 4). The adsorption capacity decreased with the increase of the amount of adsorbent and then reached a plateau. It can have two reasons: first, by increasing the amount of adsorbent, the active sites of adsorbent remain unsaturated during the adsorption of MB onto nanocomposites, and second, at high dosages of nanocomposites, particulate

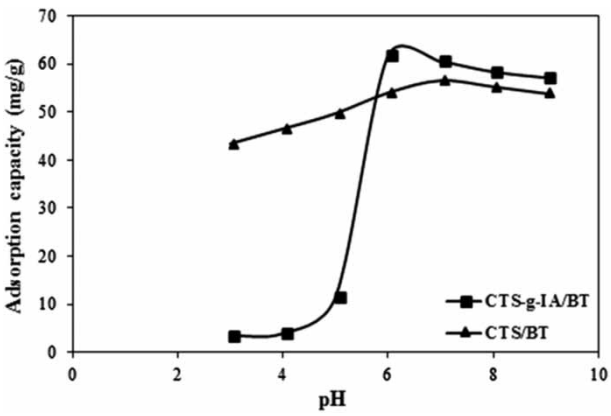

Figure 3 | The effect of the initial pH of MB solution on MB removal by CTS-g-IA/BT and CTS/BT nanocomposites (adsorbent amount = 0.03 g, initial dye concentration = 50 mg/L, contact time = 76 h, stirring rate = 120 rpm, volume of solution = 50 mL).

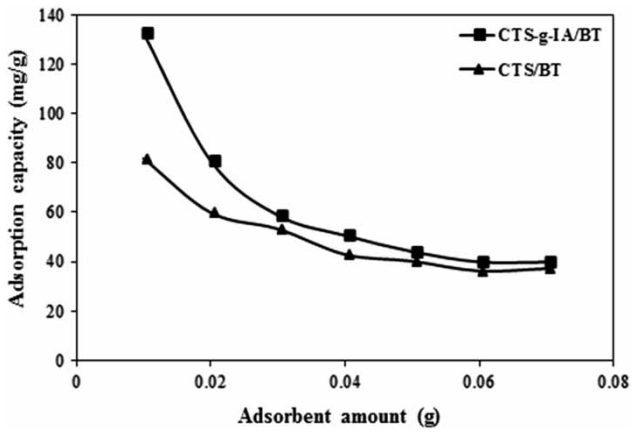

Figure 4 | The effect of adsorbent amount on MB removal by CTS-g-IA/BT and CTS/BT nanocomposites (initial dye concentration = 50 mg/L, contact time = 76 h, stirring rate = 120 rpm, volume of solution = 50 mL).

interaction like agglomeration causes a reduction in the adsorption capacity (Patel & Patel 2012).

Equilibrium studies

The experimental results of different isotherms at three temperatures (25, 35 and 40 °C) are shown in Table 1. Based on the calculated correlation coefficient (R^2) values, among the investigated isotherm models, the Langmuir equation (with the R^2 values of 0.9997 and 0.9998 for CTS/BT and CTS-g-IA/BT nanocomposites, respectively) suggested the best fitness for adsorption of MB dye with the maximum adsorption capacity of 181.82 and 500 mg/g for CTS/BT and CTS-g-IA/BT nanocomposites at 40 °C, respectively. It was observed that maximum adsorption capacity for CTS-g-IA/BT nanocomposite was higher than that for CTS/BT nanocomposite at three studied temperatures; it can be related to the double carboxylic acid groups of itaconic acid, which adsorbed more MB molecules (Ozkahraman *et al.* 2011). Based on the calculated R_L values that were less than 1, the adsorption of MB in all the investigated initial concentrations and temperatures for both nanocomposites was favorable, and the MB adsorption in higher initial dye concentration was better (Table 1). The R^2 values of Freundlich isotherm for CTS/BT and CTS-g-IA/BT nanocomposites were poorer than those for Langmuir; thus, adsorption of MB on adsorbent is not done in multilayer. It is obvious that the adsorbent can be employed in all concentrations of the adsorbate based on the calculated *1/n* values (Table 1). The values of q_D and E in three temperatures (25, 35 and 40 °C) calculated from D-R isotherm are shown in Table 1. Difference between the maximum adsorption capacity values (q_D) in the D-R isotherm and Langmuir isotherm models can be attributed to various assumptions considered during the formulations. According to the calculated E values that were less than 8 kJ/mol, the adsorption process is a physical sorption.

The maximum adsorption capacity for removal of MB by CTS-g-IA/BT and CTS/BT was compared with other nanocomposites for adsorption of MB (Table 2). The maximum adsorption capacity of synthesized nanocomposite in this study was more than in most of other adsorbents. Thus, it seems that CTS-g-IA/BT nanocomposite can be applied for removal of MB as a successful adsorbent.

Thermodynamic parameters

Thermodynamic parameters for MB adsorption onto CTS/BT and CTS-g-IA/BT nanocomposites at three

Table 1 | Parameter values of the isotherm models for MB adsorption onto CTS/BT and CTS-g-IA/BT nanocomposites at 25, 35 and 40 °C temperatures

Isotherms	Constants	25 °C		35 °C		40 °C	
		CTS/BT	CTS-g-IA/BT	CTS/BT	CTS-g-IA/BT	CTS/BT	CTS-g-IA/BT
Langmuir	q_m (mg/g)	95.238	250	153.846	384.615	181.82	500
	K_L (L/mg)	0.077	0.02934	0.0456	0.0248	0.04614	0.04504
	R^2	0.9992	0.9993	0.9977	0.999	0.9997	0.9998
	R_L	0.206–0.031	0.405–0.078	0.304–0.052	0.446–0.091	0.302–0.051	0.307–0.052
Freundlich	K_F (mg/g)	39.72	27.199	34.46	27.57	36.495	46.108
	1/n	0.1527	0.4037	0.2663	0.484	0.2898	0.4967
	R^2	0.9191	0.9194	0.9135	0.952	0.9347	0.9463
D-R	q_D (mg/g)	85.78	184.122	128.367	230.741	143.179	298.21
	K (mol^2/J^2)	2×10^{-5}	3×10^{-5}	3×10^{-5}	2×10^{-5}	2×10^{-5}	5×10^{-6}
	E (kJ/mol)	0.158	0.129	0.129	0.158	0.158	0.316
	R^2	0.8689	0.8691	0.8878	0.7826	0.7664	0.788

Table 2 | Comparison of the maximum adsorption capacity of various adsorbents for removal of MB

Adsorbent	q_m (mg/g)	Reference
Modified polysaccharide superabsorbent hydrogel	48	Paulino *et al.* (2006)
Chitosan-g-poly(acrylic acid)/montmorillonite hydrogel	1,859	Wang *et al.* (2008)
Poly(NIPAAm/AA/N-allylisatin) nanohydrogel	392.15	Mahida & Patel (2016)
Hydrolyzed polyacrylamide/cellulose nanocomposite	326.08	Zhou *et al.* (2014)
Poly(AA-co-AMPS)/montmorillonite nanocomposite	215	Hosseinzadeh & Khoshnood (2015)
Xylan/poly(acrylic acid) magnetic nanocomposite	438.6	Sun *et al.* (2015)
CTS/BT nanocomposite	181.82	Present study
CTS-g-IA/BT nanocomposite	500	Present study

temperatures (25, 35 and 40 °C) are illustrated in Table 3. Due to the negative values of the ΔG^0, the adsorption process was spontaneous, and more favorable at high temperatures. The ΔH^0 values were obtained as 15.27 and 25.666 kJ/mol for CTS/BT and CTS-g-IA/BT nanocomposites, respectively. The positive values of ΔH^0 predicted an endothermic process. The endothermic nature of the adsorption process can be explained as below: generally, adsorption is an exothermic process, but when the MB ions get to the surface, they lose their solvating water molecules; this dehydration process consumes a lot of energy, and therefore, when the amount of dehydration energy overcomes the enthalpy of the adsorption MB to the surface, the ΔH^0 value becomes positive (Wu *et al.* 2015). According to Fu *et al.* (2015) the ΔH^0 change values less than 40 kJ/mol suggest a physical adsorption (Table 3). The positive values of ΔS^0 confirm the increasing randomness of adsorption process. Possibly the higher mobility, obtained from desolvation of adsorbate ions, can increase the randomness of adsorption (Maatar & Boufi 2015).

Kinetic studies

As shown in Figure 5, at the first step of the adsorption process, due to the existence of numerous active sites on the adsorbent surface, increasing of adsorption capacity is fast; however, the rate of adsorption decreases with time. This phenomenon is related to occupying of the active sites of adsorbent with dye molecules; therefore, the available sites decrease (Liu *et al.* 2010; Wu *et al.* 2015). The removal efficiency of MB at the first 24 h was 50%. Finally, the adsorption capacity of MB onto the CTS/BT and CTS-g-IA/BT nanocomposites reached equilibrium state. The equilibrium time for MB removal was determined as 76 h. It seems that the equilibrium time is very long. It can be interpreted with two reasons, as follows. (1) The rate of stirring in the present work was slow (120 rpm). By increasing the stirring rate, because of enhancement of the turbulence and decrease of the thickness of the liquid boundary layer, adsorption of MB enhances (Hanafiah *et al.* 2012). (2) The long equilibrium time can be related to the existence of BT in the nanocomposites structure. By adding clay into the structure of hydrogel, the strength property of nanocomposites enhances (Haraguchi 2007). On the other hand, the presence of BT in the structure of nanocomposite can decrease the diffusion of MB molecules into the adsorbent (Wang *et al.* 2009).

The results of kinetic models are shown in Table 4. It implies that pseudo-first-order model is not a favorable kinetic model for removal of MB onto the nanocomposites due to the poor correlation coefficient values (R^2). The experimental adsorption kinetic data showed that the correlation coefficient values for pseudo-second-order had better fitness among the other studied kinetic models. Figure 6 illustrated the bi-linear plots of intraparticle diffusion model for the two adsorbents. Many steps like film

Table 3 | Thermodynamic parameters for MB adsorption onto CTS/BT and CTS-g-IA/BT nanocomposites at three temperatures (25, 35 and 40 °C)

	CTS/BT			CTS-g-IA/BT		
Parameters	25 °C	35 °C	40 °C	25 °C	35 °C	40 °C
K_0	1.3197	1.5744	1.7845	1.7478	2.1095	2.9876
ΔG^0(kJ/mol)	−0.687	−1.162	−1.507	−1.383	−1.9111	−2.84
ΔH^0(kJ/mol)		15.27			25.666	
ΔS^0(J/mol K)		53.503			90.448	

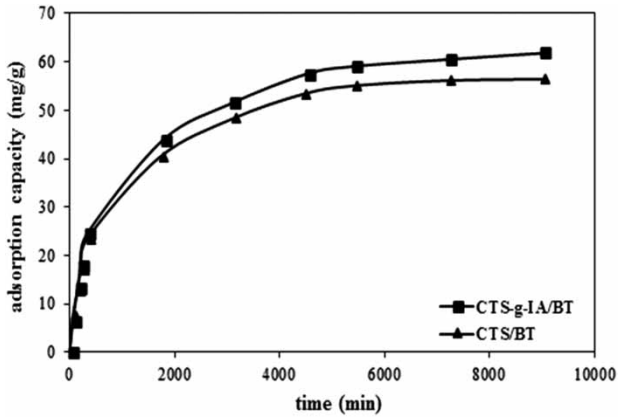

Figure 5 | The effect of contact time on MB removal by CTS-g-IA/BT and CTS/BT nanocomposites (adsorbent amount = 0.03 g, initial dye concentration = 50 mg/L, stirring rate = 120 rpm, volume of solution = 50 mL).

Table 4 | Constants of kinetic models for MB adsorption onto CTS/BT and CTS-g-IA/BT nanocomposites at 25 °C, 120 rpm

			Adsorbent name	
	Parameters		CTS/BT	CTS-g-IA/BT
Models	qe, exp (mg/g)		56.41	61.79
Pseudo-first-order model	$q_e$cal (mg/g)		50.9	49.46
	k_1 (1/min)		0.00069	0.0004606
	R^2		0.9902	0.9952
Pseudo-second-order model	$q_e$cal (mg/g)		60.24	65.35
	k_2 (g/mg min)		0.000027	0.000024
	R^2		0.9977	0.9979
Intraparticle diffusion model		k_{i1}	0.9467	1.0412
	Step 1	I	1.7792	1.405
		R^2	0.9875	0.9595
		k_{i2}	0.2683	0.3059
	Step 2	I	34.345	35.626
		R^2	0.8865	0.8913

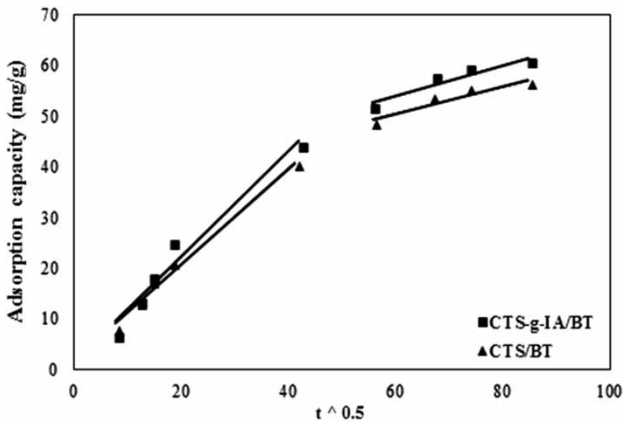

Figure 6 | The intraparticle diffusion kinetic model.

diffusion, intraparticle diffusion, and chemical reaction on the adsorbent can control the adsorption process. As shown, the first step, which is the transfer of MB molecules from the solution toward the adsorbent surface (film diffusion), is faster than the other step, so that diffusing the adsorbate molecules into the adsorbent is more difficult. Table 4 shows the k_i and I values for both adsorbents. According to the experimental data, k_i values for CTS-g-IA/BT nanocomposite were higher than for CTS/BT nanocomposite, indicating that the initial rates of MB adsorption on CTS-g-IA/BT were higher than those on CTS/BT.

CONCLUSION

In the present study, CTS/BT and CTS-g-IA/BT nanocomposites were synthesized using free radical polymerization for MB adsorption from aqueous solution. The experimental results illustrated that the adsorption capacity decreased with an increment of adsorbent amount; however, it increased by an increment of pH and contact time. The optimum pH for the adsorption capacity of CTS/BT and CTS-g-IA/BT nanocomposites was obtained as 7 and 6, respectively. In all experiments, CTS-g-IA/BT nanocomposite had the higher adsorption capacity compared to CTS/BT nanocomposite due to the existence of carboxyl functional groups. The equilibrium data followed Langmuir isotherm model with maximum adsorption capacities of 181.82 and 500 mg/g for CTS/BT and CTS-g-IA/BT nanocomposites, respectively. The kinetic adsorption data showed that the required equilibrium time for adsorption of MB was 76 h for both nanocomposites. Pseudo-second-order model fitted the kinetic data well. The negative values of standard Gibbs free energy (ΔG^0) for both adsorbents suggested a spontaneous process. The values of the standard enthalpy (ΔH^0) were obtained as 15.27 and 25.666 kJ/mol for CTS/BT and CTS-g-IA/BT nanocomposites, respectively. Not only did the positive values of ΔH^0 show an endothermic adsorption, but also the values less than 40 kJ/mol confirmed the physical adsorption. Increasing the randomness on the surface of adsorbents was confirmed by positive values of the standard entropy (ΔS^0) for both nanocomposites.

REFERENCES

Aflaki Jalali, M., Dadvand Koohi, A. & Sheykhan, M. 2016 Experimental study of the removal of copper ions using

hydrogels of xanthan, 2-acrylamido-2-methyl-1-propane sulfonic acid, montmorillonite: kinetic and equilibrium study. *Carbohydrate Polymers* **142**, 124–132.

Auta, M. & Hameed, B. H. 2014 Chitosan–clay composite as highly effective and low-cost adsorbent for batch and fixed-bed adsorption of methylene blue. *Chemical Engineering Journal* **237**, 352–361.

Bao, Y., Ma, J. & Li, N. 2011 Synthesis and swelling behaviors of sodium carboxymethyl cellulose-g-poly(AA-co-AM-co-AMPS)/MMT superabsorbent hydrogel. *Carbohydrate Polymers* **84**, 76–82.

Dang, V. B. H., Doan, H. D., Dang-Vu, T. & Lohi, A. 2009 Equilibrium and kinetics of biosorption of cadmium(II) and copper(II) ions by wheat straw. *Bioresource Technology* **100** (1), 211–219.

Fu, J., Chen, Z., Wang, M., Liu, S., Zhang, J., Zhang, J., Han, R. & Xu, Q. 2015 Adsorption of methylene blue by a high-efficiency adsorbent(polydopamine microspheres): kinetics, isotherm, thermodynamics and mechanism analysis. *Chemical Engineering Journal* **259**, 53–61.

Guclu, G., Al, E., Emik, S., Iyim, T. B., Ozgumus, S. & Ozyurek, M. 2010 Removal of Cu^{2+} and Pb^{2+} ions from aqueous solutions by starch-graft-acrylic acid/montmorillonite superabsorbent nanocomposite hydrogels. *Polymer Bulletin* **65** (4), 333–346.

Hanafiah, M. A. K. M., Ngah, W. S. W., Zolkafly, S. H., Teong, L. C. & Abdul Majid, Z. A. 2012 Acid Blue 25 adsorption on base treated *Shorea dasyphylla* sawdust: kinetic, isotherm, thermodynamic and spectroscopic analysis. *Journal of Environmental Sciences* **24** (2), 261–268.

Haraguchi, K. 2007 Nanocomposite hydrogels. *Current Opinion in Solid State and Materials Science* **11**, 47–54.

He, Y. F., Zhang, L., Yan, D. Z., Liu, S. L., Wang, H., Li, H. R. & Wang, R. M. 2012 Poly(acrylic acid) modifying bentonite with in-situ polymerization for removing lead ions. *Water Science & Technology* **65** (8), 1383–1391.

Hosseinzadeh, H. & Khoshnood, N. 2015 Removal of cationic dyes by poly(AA-co-AMPS)/montmorillonite nanocomposite hydrogel. *Desalination and Water Treatment* **57** (14), 6372–6383.

Kaplan, M. & Kasgoz, H. 2011 Hydrogel nanocomposite sorbents for removal of basic dyes. *Polymer Bulletin* **67**, 1153–1168.

Kumar, M. & Tamilarasan, R. 2013 Modeling studies for the removal of methylene blue from aqueous solution using Acacia fumosa seed shell activated carbon. *Journal of Environmental Chemical Engineering* **1** (4), 1108–1116.

Krdtabar, M., Peyvand Kermani, Z. & Bagheri Marandi, G. 2015 Synthesis and characterization of collagen-based hydrogel nanocomposites for adsorption of Cd^{2+}, Pb^{2+}, methylene green and crystal violet. *Iranian Polymer Journal* **24** (9), 791–803.

Liu, Y., Wang, W. & Wang, A. 2010 Adsorption of lead ions from aqueous solution by using carboxymethyl cellulose-g-poly (acrylic acid)/attapulgite hydrogel composites. *Desalination* **259**, 258–264.

Maatar, W. & Boufi, S. 2015 Poly(methacylic acid-co-maleic acid) grafted nanofibrillated cellulose as a reusable novel heavy metal ions adsorbent. *Carbohydrate Polymers* **126**, 199–207.

Mahida, V. P. & Patel, M. P. 2016 Removal of some most hazardous cationic dyes using novel poly (NIPAAm/AA/N-allylisatin) nanohydrogel. *Arabian Journal of Chemistry* **9** (3), 430–442.

Merzouk, B., Madani, K. & Sekki, A. 2010 Using electrocoagulation–electroflotation technology to treat synthetic solution and textile wastewater, two case studies. *Desalination* **250**, 573–577.

Milosavljevic, N. B., Ristic, M. Đ., Peric-Grujic, A. A., Filipovi, J. M., Strbac, S. B., Rakocevic, Z. L. & Kalagasidis Krusic, M. T. 2010 Hydrogel based on chitosan, itaconic acid and methacrylic acid as adsorbent of Cd^{2+} ions from aqueous solution. *Chemical Engineering Journal* **165**, 554–562.

Mittal, H., Parashar, V., Mishra, S. B. & Mishra, A. K. 2014 Fe_3O_4 MNPs and gum xanthan based hydrogels nanocomposites for the efficient capture of malachite green from aqueous solution. *Chemical Engineering Journal* **255**, 471–482.

Moussout, H., Ahlafi, H., Aazza, M., Zegaoui, O. & El Akili, C. 2016 Adsorption studies of Cu(II) onto biopolymer chitosan and its nanocomposite 5% bentonite/chitosan. *Water Science & Technology* **73** (9), 2199–2210.

Ozkahraman, B., Acar, I. & Emik, S. 2011 Removal of cationic dyes from aqueous solutions with poly (N-isopropylacrylamide-co-itaconic acid) hydrogels. *Polymer Bulletin* **66** (4), 551–570.

Patel, Y. N. & Patel, M. P. 2012 Novel cationic poly[AAm/NVP/DAPB] hydrogels for removal of some textile anionic dyes from aqueous solution. *Journal of Macromolecular Science-Pure and Applied Chemistry* **49** (6), 490–501.

Paulino, A. T., Guilherme, M. R., Reis, A. V., Campese, G. M., Muniz, E. C. & Nozaki, J. 2006 Removal of methylene blue dye from an aqueous media using superabsorbent hydrogel supported on modified polysaccharide. *Journal of Colloid and Interface Science* **301** (1), 55–62.

Pourjavadi, A., Mazaheri Tehrani, Z., Salimi, H., Banazadeh, A. & Abedini, N. 2015 Hydrogel nanocomposite based on chitosan-g-acrylic acid modified nanosilica with high adsorption capacity for heavy metal ion removal. *Iranian Polymer Journal* **24** (9), 725–734.

Salama, A., Shukry, N. & El-Sakhawy, M. 2014 Carboxymethyl cellulose-g-poly(2-(dimethylamino)ethyl methacrylate) hydrogel as adsorbent for dye removal. *International Journal of Biological Macromolecules* **73**, 72–75.

Sharma, R., Kaith, B. S., Kalia, S., Pathania, D., Kumar, A., Sharma, N., Street, R. M. & Schauer, C. 2015 Biodegradable and conducting hydrogels based on Guar gum polysaccharide for antibacterial and dye removal applications. *Journal of Environmental Management* **162**, 37–45.

Shirsath, S. R., Hage, A. P., Zhou, M., Sonawane, S. H. & Ashokkumar, M. 2011 Ultrasound assisted preparation of nanoclay Bentonite-FeCo nanocomposite hybrid hydrogel: a potential responsive sorbent for removal of organic pollutant from water. *Desalination* **281**, 429–437.

Shivarkar, A. B., Gaykar, D. V. & Jain, R. K. 2015 Study of performance properties of itaconic acid based acrylic-modified polyester for industrial baking finishes. *Progress in Organic Coatings* **89**, 75–81.

Sun, X. F., Liu, B., Jing, Z. & Wang, H. 2015 Preparation and adsorption property of xylan/poly(acrylic acid)magnetic nanocomposite hydrogel adsorbent. *Carbohydrate Polymers* **118**, 16–23.

Tabrizi, N. S. & Yavari, M. 2015 Methylene blue removal by carbon nanotube-based aerogels. *Chemical Engineering Research and Design* **94**, 516–523.

Tahri, N., Masmoudi, G., Ellouze, E., Jrad, A., Drogui, P. & Amar, R. B. 2012 Coupling microfiltration and nanofiltration processes for the treatment at source of dyeing-containing effluent. *Journal of Cleaner Production* **33**, 226–235.

Wang, L., Zhang, J. & Wang, A. 2008 Removal of methylene blue from aqueous solution using chitosan-g-poly(acrylic acid)/montmorillonite superadsorbent nanocomposite. *Colloids and Surfaces A: Physicochemical and Engineering Aspects* **322** (1–3), 47–53.

Wang, X., Zheng, Y. & Wang, A. 2009 Fast removal of copper ions from aqueous solution by chitosan-g-poly(acrylic acid)/attapulgite composites. *Journal of Hazardous Materials* **168**, 970–977.

Wang, X., Yang, L., Zhang, J., Wang, C. & Li, Q. 2014 Preparation and characterization of chitosan–poly(vinyl alcohol)/bentonite nanocomposites for adsorption of Hg(II) ions. *Chemical Engineering Journal* **251**, 404–412.

Wu, X. P., Xu, Y. Q., Zhang, X. L., Yu-cheng Wu, Y. C. & Gao, P. 2015 Adsorption of low-concentration methylene blue onto a playgorskite/carbon composite. *New Carbon Materials* **30** (1), 71–78.

Yang, X. & Ni, L. 2012 Synthesis of hybrid hydrogel of poly(AM co DADMAC)/silica sol and removal of methyl orange from aqueous solutions. *Chemical Engineering Journal* **209**, 194–200.

Zhang, J., Wang, L. & Wang, A. 2007 Preparation and properties of chitosan-g-poly(acrylic acid)/montmorillonite superabsorbent nanocomposite via in situ intercalative polymerization. *Industrial & Engineering Chemistry Research* **46** (8), 2497–2502.

Zheng, Y. & Wang, A. 2009 Evaluation of ammonium removal using a chitosan-g-poly (acrylic acid)/rectorite hydrogel composite. *Journal of Hazardous Materials* **171** (1–3), 671–677.

Zhou, C., Wua, Q., Lei, T. & Negulescu, I. I. 2014 Adsorption kinetic and equilibrium studies for methylene blue dye by partially hydrolyzed polyacrylamide/cellulose nanocrystal nanocomposite hydrogels. *Chemical Engineering Journal* **251**, 17–24.

First received 29 June 2016; accepted in revised form 26 January 2017. Available online 10 February 2017